Kinetic-energy distributions of positive and negative ions in Townsend discharges in oxygen

M. V. V. S. Rao,* R. J. Van Brunt,[†] and J. K. Olthoff[‡]

Electronics and Electrical Engineering Laboratory, National Institute of Standards and Technology, Gaithersburg, Maryland 20899-8113

(Received 16 November 1998)

Translational flux-energy distributions of positive and negative ions have been measured at high electric field-to-gas density ratios (E/N) up to 40×10^{-18} V m^2 (40 kTd) in diffuse, parallel-plate Townsend discharges in oxygen using an ion energy analyzer-mass spectrometer. The O_2^+ ion is the most abundant ion detected in the discharge, and exhibits Maxwellian energy distributions for $E/N<20\times10^{-18}$ V m^2, which is consistent with predictions based upon the assumption that resonant symmetric charge exchange is the dominant ion-molecule collision process. The less abundant ions O^+, O_2^-, and O^- exhibit non-Mawellian ion kinetic-energy distributions at nearly all E/N, indicative of multiple ion-molecule reactions affecting the ion transport. Mean energies are obtained for each ion as a function of E/N from an analysis of the energy distributions, and symmetric charge-exchange cross sections are calculated from the data where appropriate. [S1063-651X(99)09304-6]

PACS number(s): 52.20.Hv, 52.80.$-$s, 52.25.Fi

I. INTRODUCTION

Understanding the details of ion production and transport in electrical discharges is of importance to both the semiconductor industry, which uses gas-phase discharges for microelectronic device production, and the electric equipment industry, which uses electronegative gases as high voltage insulation. Oxygen is a gas of interest to both of these areas due to its common usage in plasma discharges for etching and cleaning processes, and its nearly universal presence as an impurity in high voltage insulation systems.

Numerous studies of ion transport in oxygen have been published over the years, primarily presenting data related to ion mobilities and drift velocities [1], and a single paper presents measurements of ion-energy distributions in oxygen [2]. However, all of this previous work deals with conditions where the density-reduced electric field (electric field-to-gas density ratio, E/N) is less than 600×10^{-21} V m^2 (600 Td). In this paper, we utilize a dc Townsend discharge to measure the energy distribution of positive and negative ions striking the grounded electrode for values of E/N ranging from 2 $\times10^{-18}$ to 40×10^{-18} V m^2 (2–40 kTd). These values of E/N are comparable to those observed in the sheath regions of glow discharges used in plasma processing applications, and the information about ion-molecule reactions derived from these investigations is relevant to the analysis of ion-energy distributions measured in rf plasma discharges (see, for example, Refs. [3,4]).

Analysis of the identity, energies, and intensities of the ions generated in a discharge permits a qualitative analysis of the ion-production processes and subsequent ion-molecule collision processes that affect the flux of ions through the discharge. Additionally, analysis of the energy distributions allows a determination of the range of E/N for which equilibrium conditions exist (i.e., conditions for which an ion experiences many collisions during its transit across the discharge gap, essentially eliminating any dependence of its energy upon its point of formation). This information, while measured here for a simple dc parallel-plate discharge, is useful in the modeling of more complex discharges.

In this paper we report ion-flux energy distributions (IFED's) for O_2^+, O^+, O_2^-, and O^- ions striking the grounded electrode of a low current, diffuse, dc Townsend discharge in oxygen. The importance of various ion-molecule reactions are discussed based upon the shape of the measured IFED's, and the mean energies are calculated for each distribution, which are related to drift velocity measurements and, in some cases, effective charge-exchange cross sections.

II. EXPERIMENT

A. Apparatus

The experimental apparatus used here is essentially the same as used previously [5] in our studies of Townsend discharges in rare gases. Briefly, the discharge cell consists of two flat, parallel, 11-cm-diameter stainless steel electrodes surrounded by a cylindrical quartz tube that is uniformly separated from the outer edges of the electrode by a space of 1 mm to allow gas flow through the interelectrode gap. The interelectrode gap can be varied from 0 to 4 cm, but all data presented here were obtained with a gap spacing of 2 cm. A 0.1-mm hole is located in the center of the grounded, lower electrode in order to extract ions for mass and energy analysis. The discharge is generated by biasing the upper electrode either positively or negatively in order to sample positive or negative ions, respectively.

Ions passing through the 0.1-mm sampling orifice in the grounded electrode enter the differentially pumped ion energy analyzer-mass spectrometer system and are energy and mass analyzed. This device has been described previously [5,6]. It basically consists of a 45° electrostatic ion-energy selector coupled to a quadrupole mass spectrometer. The resolution of the mass spectrometer was approximately 1 u

*Present address: MS 229-1, NASA/Ames Research Center, Moffet Field, CA 94035.
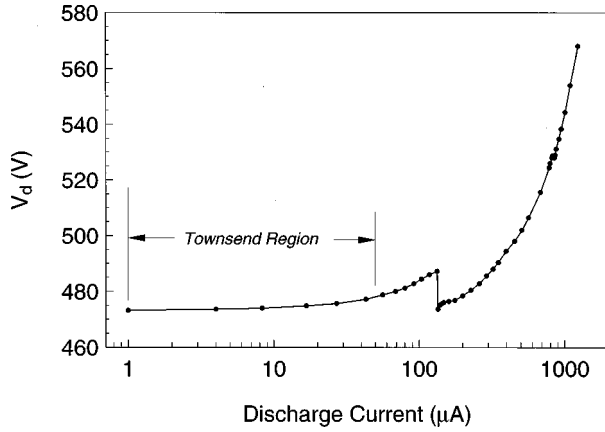
[†]Retired.

[‡]Electronic address: james.olthoff@nist.gov

FIG. 1. Voltage-current characteristic curve measured for an oxygen discharge at $E/N = 5 \times 10^{-18}$ V m^2 (5 kTd) at a gap spacing of 2 cm.

(amu), and the resolution of the electrostatic energy analyzer was maintained at 4 eV, independent of the mass and energy of the ion.

The electric-field strength E in the discharge gap is assumed to be given by V_d/d, where d is the interelectrode gap spacing (2 cm for all data presented here), and V_d is the voltage drop across the gap measured by a voltmeter. This assumption is valid in the Townsend discharges studied here because the current densities are too low to significantly affect the applied electric field. The gas density N is determined from the gas pressure in the gap region as measured by a capacitive manometer (baratron). The combined error of these measurements indicates that the uncertainty in the measured E/N of a discharge is $\pm 3\%$.

An example of the voltage-current characteristic curve for oxygen in this discharge cell is shown in Fig. 1. The Townsend region is designated in the figure, and corresponds to the region where the discharge voltage V_d is nearly independent of discharge current. The external circuitry used to apply the voltage to the powered electrode was designed to produce Townsend conditions over the largest range of currents possible [5]. The ion-energy data presented here were all obtained at discharge currents between 10 and 20 μA. Near 100 μA the discharge became unstable (as evidenced by the discontinuity in the IV curve) before transitioning into a stable glow discharge at higher currents. Another smaller region of instability was observed at currents near 800 μA.

B. Data analysis

As discussed in Ref. [5], the distribution function $F(\varepsilon)$ of the ion kinetic energies that is measured by this experiment is the *ion-flux energy distribution*, i.e., the number of ions per second with energy between ε and $\varepsilon + d\varepsilon$ that strike a particular area of the lower electrode [7]. Under certain discharge conditions the form of the IFED can be predicted from a simple one-dimensional model [5,8] based upon three basic assumptions: (1) the ion motion takes place in a constant, uniform, high electric field; (2) symmetric charge-exchange is the predominant ion-neutral interaction, and this process has a cross section σ_{CT} whose magnitude is nearly independent of collision energies; and (3) equilibrium conditions apply (i.e., the ions experience many collisions as they
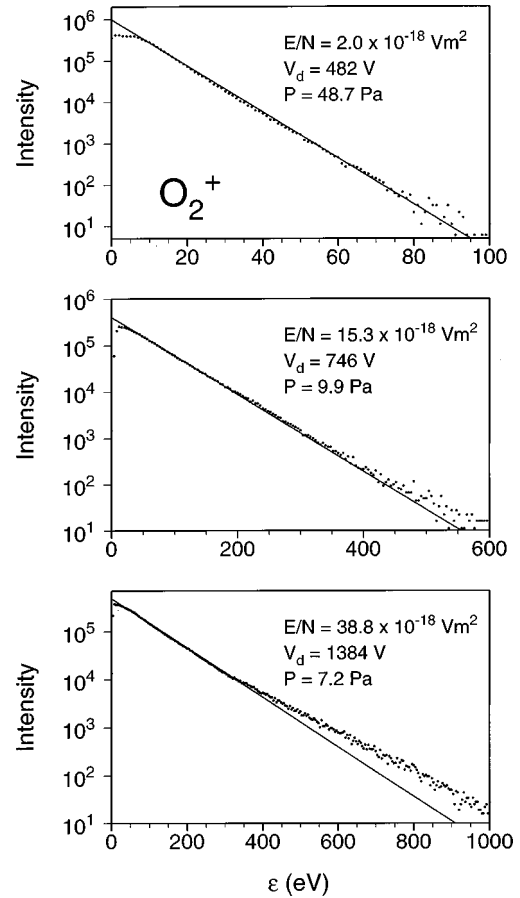

FIG. 2. Measured ion-flux energy distributions for O$_2^+$ in O$_2$ at three indicated values of E/N for a gap spacing of 2 cm. The solid lines correspond to a Maxwellian fit to the data.

travel through the discharge), so that the ion transport satisfies the one-dimensional Boltzmann transport equation. For discharges and ions conforming to these conditions, the IFED takes the Maxwellian form

$$F(\varepsilon) = \frac{1}{kT_+} \exp(-\varepsilon/kT_+), \qquad (1)$$

where ε is the ion energy, and T_+ is the "effective ion temperature" which is defined as

$$kT_+ = \frac{e}{\sigma_{CT}} \frac{E}{N}, \qquad (2)$$

where e is the electron charge. Under these conditions, the mean energy calculated from the ion-flux energy distribution, $\langle \varepsilon \rangle_F$, reduces to

$$\langle \varepsilon \rangle_F = kT_+, \qquad (3)$$

thus allowing the mean energy to be determined from the slope of the IFED when plotted on a semilog plot (as will be shown later in Fig. 2) [5]. Thus a direct proportionality exists between the mean energy and the density-reduced electric field, with an inverse proportionality existing between the mean energy and the symmetric charge-transfer cross section:

$$\langle \varepsilon \rangle_F = \frac{e}{\sigma_{\mathrm{CT}}} \frac{E}{N}. \tag{4}$$

For the case where the mass of the ion, M, is equal to the mass of the molecules in the background gas, the mean energy has been shown [5] to be related to the ion drift velocity w by the equation

$$\langle \varepsilon \rangle_F = \frac{\pi}{2} M w^2. \tag{5}$$

This simple model has been shown to describe Townsend discharges accurately in rare gases for $E/N < 20 \times 10^{-18}$ V m^2 [5,8], and, as will be discussed later in this paper, is consistent with the data for O$_2^+$ and O$_2^-$ ions in oxygen.

It is important to note that $\langle \varepsilon \rangle_F$ is the mean of the ion-flux energy distribution (i.e., the mean energy of the ion flux striking the electrode), which is not the same as the mean energy $\langle \varepsilon \rangle$ of the ions present in the discharge gap at any given time (which has been called the ''true'' mean energy and is the mean energy often referred to in drift-type experiments [9]). It can be shown that the two mean energies are related to each other by a factor of $\frac{1}{2}$ [5]:

$$\langle \varepsilon \rangle = \tfrac{1}{2} \langle \varepsilon \rangle_F. \tag{6}$$

For a discussion of the equivalent relationship between $\langle \varepsilon \rangle$ and σ_{CT} and w for the ''true'' energy distributions, the reader is referred to Refs. [9–11]. For the remainder of this paper the term ''mean energy'' will refer to $\langle \varepsilon \rangle_F$.

For ions and/or discharges that do not satisfy the three conditions discussed earlier in this section, and therefore do not exhibit a Maxwellian-shaped IFED, the mean energy must be determined by performing an energy-weighted integration of the flux-energy distribution of the form

$$\langle \varepsilon \rangle = \frac{\int \varepsilon F(\varepsilon) d\varepsilon}{\int F(\varepsilon) d\varepsilon}, \tag{7}$$

which for our experimental data can be written

$$\langle \varepsilon \rangle = \frac{\sum_i \varepsilon_i S_i}{\sum_i S_i}, \tag{8}$$

where ε_i and S_i are the energy and number of counts corresponding to the ith channel of the ion-flux energy distribution obtained by the energy scan of the ion-energy analyzer-mass spectrometer (IEA-MS).

Detailed investigation of the transmission characteristics of the IEA-MS system indicates that the ion-energy distribution data are less reproducible at energies below 10 eV. This is indicative of low-energy discrimination resulting primarily from the charging of surfaces near the sampling orifice [12,13]. Calculation of the mean ion energy for a measured distribution using Eq. (8) can result in an overdetermination of up to 20% due to loss of signal at low energies. The

effects of this discrimination on the calculation of the mean energies can be compensated for, in cases where the ion-energy distribution is linear at low energies, by extrapolating the intensity of the distributions down to 0 eV. In general, calculated values of $\langle \varepsilon \rangle_F$ are reproducible to within $\pm 10\%$, with an additional uncertainty of $+20\%$ for distributions where it is not reasonable to adjust for the low-energy discrimination.

III. RESULTS

A. Kinetic-energy distributions

Ion-energy flux distributions were measured for O$_2^+$, O$^+$, O$_2^-$, and O$^-$ ions produced in the Townsend discharges. These were the only ions detected from the discharge. No evidence of O$_4^+$, O$_3^-$, or O$_4^-$ was detected even though these ions have previously been detected in drift tubes and in lower-E/N discharges [2,14–16]. If one assumes that the detection efficiencies of the mass spectrometer are approximately equal for both positive and negative ions, then the relative order of detected flux intensities is

$$[\mathrm{O}_2^+] > [\mathrm{O}^+] > [\mathrm{O}_2^-] > [\mathrm{O}^-]$$

for all E/N. However, since the relative detection efficiency of the positive and negative ions has not been confirmed, only the relative intensities of ions with the same charge will be presented later in this paper.

Examples of ion-energy flux distributions for O$_2^+$ ions are shown in Fig. 2 for three widely separated values of E/N ranging from 2×10^{-18} V m^2 (2 kTd) to nearly 40×10^{-18} V m^2 (40 kTd). For values of $E/N \leq 15 \times 10^{-18}$ V m^2, the distributions are Maxwellian in shape, except for the effects of low-energy discrimination observed below 10 eV. The solid line in each figure represents the fit to the data above 10 eV, the slope of which can be used to determine the mean energy of the distributions (as discussed in Sec. II). The Maxwellian shape of the IFED's in Fig. 2 are consistent with symmetric charge exchange being the dominant collision process affecting the transport of O$_2^+$ ions in O$_2$.

Above 15×10^{-18} V m^2 the ion kinetic-energy distributions deviate from the Maxwellian form, as is evident by the ''two-temperature'' behavior of the distribution shown at the bottom of Fig. 2 for $E/N = 38.8 \times 10^{-18}$ V m^2. The solid line is a fit to the linear portion of the distribution from approximately 50 to 300 eV, and is used to extrapolate the distribution down to 0 eV in order to minimize the effects of low-energy discrimination on the calculation of mean energies using Eq. (8) (as discussed in Sec. II). The E/N dependence of the IFED's for O$_2^+$ in O$_2$ is similar to that observed for rare gases [5], which is expected since O$_2^+$ in oxygen exhibits a symmetric charge-exchange cross section that is similar in magnitude to those of rare gas ions. The shapes of the O$_2^+$ IFED's for E/N above 15×10^{-18} V m^2 are not fully understood, but may be attributed to the advent of nonequilibrium conditions (at the lowest pressures used here, rough estimates indicate a mean free path of approximately 0.1 cm [9]), or to increasing contributions from collisions other than symmetric charge transfer as the ion energies increase.
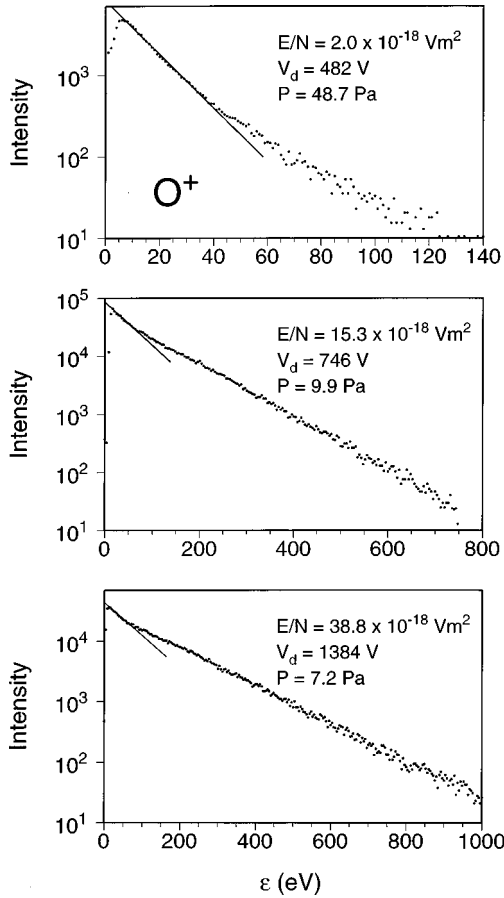
FIG. 3. Measured ion-flux energy distributions for O^+ in O_2 at three indicated values of E/N for a gap spacing of 2 cm. The solid lines correspond to linear fits at energies just above 10 eV used to correct for low-energy ion discrimination.

Shown in Fig. 3 are three ion-flux energy distributions for O^+ ions at the same values of E/N used for the O_2^+ data in Fig. 2. The IFED's for O^+ are non-Maxwellian in shape at all E/N, showing minor deviations from linear behavior on the semilog plots. The short lines are fits to the lower-energy portion of the distributions, allowing extrapolation down to 0 eV to minimize the effects of low-energy discrimination. The deviations of the data from the lines at higher energies clearly show the ''two-temperature'' behavior observed at all E/N. The maximum energy of the O^+ ions exceed those of the O_2^+ ions at the same values of E/N, and, at the higher values of E/N, extend to the maximum kinetic energies possible for the applied gap voltage.

Representative IFED's for O_2^- and O^- ions are shown in Figs. 4 and 5, respectively, for values of E/N ranging from 3×10^{-18} to 30×10^{-18} V m^2 (3–30 kTd). With the exception of O_2^- at 3×10^{-18} V m^2, the energy distributions deviate significantly from Maxwellian shape for both ions at all E/N, indicating the influence of ion-molecule reactions other than symmetric charge exchange in the formation and transport of the ions across the gap. Additionally, the maximum energies observed in the distributions for the negative ions are substantially lower than the maximum ion energies exhibited by their positive ion counterparts, which suggests the possible influence of destructive ion-molecule reactions such as collisional detachment during the transport of the negative ions across the discharge gap.
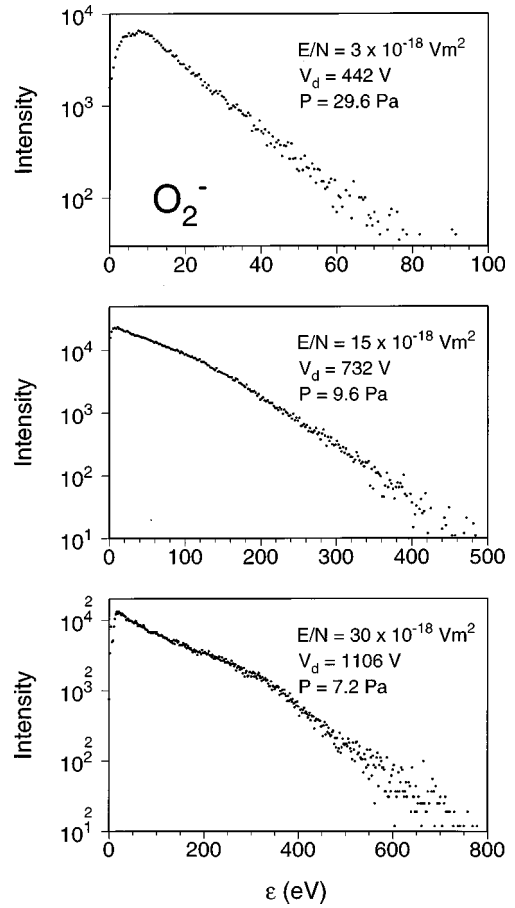

FIG. 4. Measured ion-flux energy distributions for O_2^- in O_2 at three indicated values of E/N for a gap spacing of 2 cm.

B. Mean energies $\langle \varepsilon \rangle_F$

Shown in Fig. 6(a) are the mean energies $\langle \varepsilon \rangle_F$ for the positive ions O_2^+ and O^+, derived from the ion-flux energy distributions shown in Figs. 2 and 3, and also from distributions measured at other values of E/N that are not shown in the figures. For O_2^+ and O^+ the mean energies presented here were calculated using Eq. (8), but with the low-energy portion of the distribution modified by extrapolating down to 0 eV along a linear fit to the data (as discussed in Sec. II B). For the distributions exhibiting a Maxwellian shape (O_2^+ below 20×10^{-18} V m^2), this is equivalent to determining $\langle \varepsilon \rangle_F$ from kT_+, i.e., the slope of the IFED's, as shown in Fig. 2. The error bars in Fig. 6(a) are indicative of the $\pm 10\%$ reproducibility discussed previously.

The mean energies for the negative ions are shown in Fig. 6(b), as a function of E/N. These values of $\langle \varepsilon \rangle_F$ are calculated directly from the measured ion-flux energy distributions using Eq. (8), with no extrapolation down to 0 eV. This method was used due to the highly nonlinear shape of the distributions, which made it difficult to make a simple extrapolation down to low energies. The error bars shown represent the $\pm 10\%$ scatter in the measured data, although all the mean energies calculated for the negative ions must be considered upper limits due to the potential for over determination due to low-energy discrimination (up to 20%). The calculated values of $\langle \varepsilon \rangle_F$ for each ion over a range of E/N are presented in Table I.
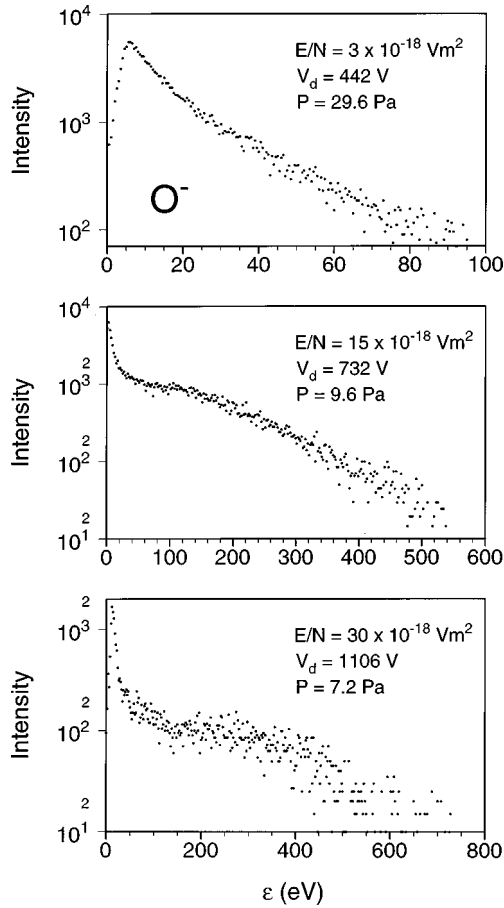
FIG. 5. Measured ion-flux energy distributions for O^- in O_2 at three indicated values of E/N for a gap spacing of 2 cm.

The dashed lines in Fig. 6 are linear fits to the data for O_2^+ and O_2^- based upon the expected proportionality between $\langle \varepsilon \rangle$ and E/N described by Eq. (4), for the conditions presented in Sec. II B. The agreement indicates consistency with these assumptions for O_2^+ for $E/N < 20 \times 10^{-18}$ V m^2 and for O_2^- for $E/N < 6 \times 10^{-18}$ V m^2. The similar linear dependence of the mean energies as a function of E/N exhibited by O^+ and O^- is simply fortuitous, since no symmetric charge-exchange processes exist for these ions under the present conditions where the concentration of O atoms is very small. Additionally, the ion-flux energy distributions clearly show evidence of other significant ion-molecule reaction for O^+ and O^- .

The calculated values of $\langle \varepsilon \rangle_F$ for rare gases have been shown to be in good agreement [5] with values calculated using drift-velocity data measured elsewhere, and with Eq. (5). However, the only drift-velocity or ion-mobility data [15–20] available for O_2^+, O^+, O_2^-, and O^- ions in O_2 are for values of E/N less than 600×10^{-21} V m^2 (600 Td). At 500×10^{-21} V m^2 values of $\langle \varepsilon \rangle_F$ calculated from these drift-velocity and ion-mobility measurements of O_2^+ [using Eq. (5)] are in reasonable agreement with an extrapolation of the dashed line in Fig. 6(a) down to low E/N (not shown on the figure). For O_2^-, the calculated values of $\langle \varepsilon \rangle_F$ from drift tube measurements at 500×10^{-21} V m^2 fall below an extrapolation of the dashed line in Fig. 6(b), in agreement with the overdetermination of $\langle \varepsilon \rangle_F$ from the measured IFED's due to low-energy discrimination.
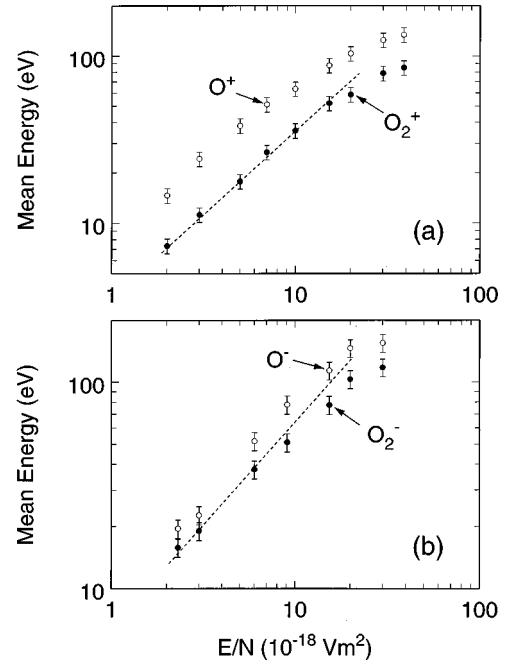

FIG. 6. Mean energies $\langle \varepsilon \rangle_F$ vs E/N for (a) O_2^+ and O^+ and (b) O_2^- and O^- in O_2. The values for the positive ions were calculated from the measured ion-flux energy distributions with compensation for low-energy discrimination. The values for the negative ions were calculated from the measured ion-flux energy distributions with no correction for low-energy discrimination. The straight lines are a reference with a slope of one.

C. Relative abundance of ions

For the data presented here, the mass spectrometer was tuned to minimize any mass discrimination over the mass range of 10–40 u. Integration of the IFED's obtained under the same discharge conditions indicate that O_2^+ is the dominant ion formed. The absolute intensity of all ions increased with increasing E/N when the ion signals were normalized by the measured current.

The relative intensities of atomic to diatomic ions of the same charge are shown in Fig. 7 as a function of E/N. These

TABLE I. Mean kinetic energies $\langle \varepsilon \rangle_F$ for the four ions generated in oxygen Townsend discharges as a function of E/N.

E/N $(10^{-18}$ V m$^2)$	$O_2^{+\,a}$ (eV)	$O^{+\,a}$ (eV)	E/N $(10^{-18}$ V m$^2)$	$O_2^{-\,b}$ (eV)	$O^{-\,b}$ (eV)
2.0	7.3	14.6	2.3	15.8	19.5
3.0	11.2	24.2	3.0	19.0	22.6
5.0	17.7	38.0	6.0	37.7	51.6
7.0	26.5	51.0	9.1	51.0	77.6
10.0	35.6	63.2	15.4	77.3	113.5
15.3	51.9	87.5	20.0	103.0	146.0
20.0	58.5	103.3	30.0	117.5	155.0
30.0	78.5	124.5			
38.8	84.8	134.0			

[a]Determined from the ion-energy distributions with extrapolation at lower energies to correct for the effects of low-energy ion discrimination (see text).

[b]Determined from the raw ion-energy distributions with no correction for low-energy ion discrimination.
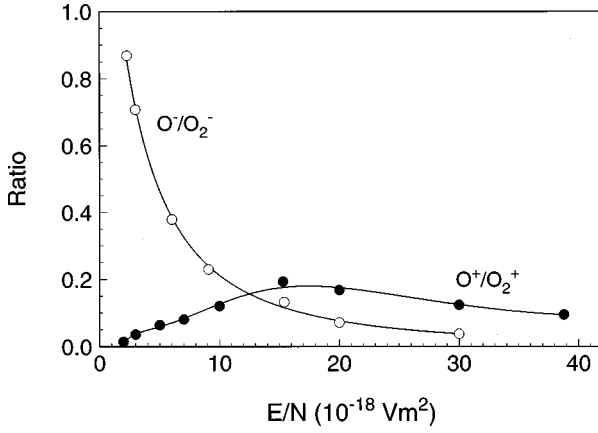
FIG. 7. Dependence of the ratio of atomic to molecular ions in oxygen on E/N.

data show that the intensity of O^- is nearly equal to that of O_2^- at low E/N, but decreases to less than 10% at higher E/N. The ratio of O^+ to O_2^+ is low at 2×10^{-18} V m^2, and then increases to a peak near 15×10^{-18} V m^2, although the intensity of O^+ never exceeds 15% of the intensity of O_2^+.

IV. DISCUSSION

A. Positive ions

Listed in Table II are some of the likely collision reactions that account for the production and transport of O_2^+ and O^+ in the discharges studied here. The dominant process for ion formation is direct ionization to form O_2^+ (reaction 1), which has a cross section more than twice that of reactions 2 and 3 combined [21] that result in the formation of O^+.

Similar to rare gas ions in their parent gas [5], the IFED's for the O_2^+ ion exhibit Maxwellian behavior for values of E/N below 20×10^{-18} V m^2. As discussed previously, this is consistent with the linear shape of the IFED's shown in the semilog plots of Fig. 2, and is also consistent with the linear dependence of the mean energy as a function of E/N shown by the dashed line in Fig. 6. Both of these conditions are indicative of the direct proportionality between $\langle \varepsilon \rangle$ and E/N described by Eq. (3). This observed behavior suggests that the simple charge-exchange model described in Sec. II B may be used to describe the ion transport of O_2^+ in O_2 for values of E/N less than 20×10^{-18} V m^2. This would be ex-

TABLE II. Reactions affecting positive ion production and transport in a Townsend discharge in oxygen.

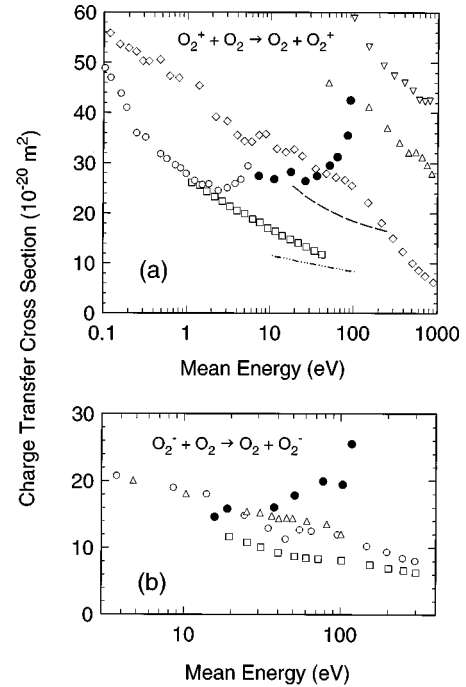|	Reaction	Process
1	$e + O_2 \rightarrow O_2^+ + 2e$	Ionization
2	$e + O_2 \rightarrow O^+ + O + 2e$	Dissociative ionization
3	$e + O_2 \rightarrow O^+ + O^- + e$	Polar dissociation
4	$O_2^+ + O_2 \rightarrow O_2 + O_2^+$	Symmetric charge exchange
5	$O_2^+ + O_2 \rightarrow O^+ + O + O_2$	Collision induced dissociation
6	$O^+ + O_2 \rightarrow O_2^+ + O$	Asymmetric charge exchange

FIG. 8. Charge-exchange cross sections ($\bullet$) calculated using Eq. (4) for (a) O_2^+ in O_2 and (b) O_2^- in O_2 compared with previously measured values from the literature. (a) $- -$, Ref. [24]; $\square$, Ref. [25]; $- \cdot \cdot -$, Ref. [28]; $\bigcirc$, Ref. [22]; $\diamond$, Ref. [23]; $\triangledown$, Ref. [26]; $\triangle$, Ref. [27]. (b) $\bigcirc$, Ref. [34]; $\square$, Ref. [33]; $\triangle$, Ref. [35].

pected since this model has been successfully applied to rare gases [5] which have charge-exchange cross sections comparable to those of O_2^+ in O_2 (reaction 4) [22–28].

For ions and discharge conditions for which the simple charge-exchange model is valid, it is possible to estimate the symmetric charge transfer cross section from Eq. (4). Figure 8(a) shows the calculated values (solid circles) of σ_{CT} for O_2^+ from the mean energy values listed in Table I. As suggested by the Maxwellian shape of the IFED's at the lower values of E/N, the calculated cross sections for E/N up to approximately 20×10^{-18} V m^2 ($\langle \varepsilon \rangle_F < 60$ eV) are in reasonable agreement with published values [22–28] for the charge-exchange cross section, although the significant scatter among the previously reported values of σ_{CT} make it difficult to determine the accuracy of the presently calculated values. The dramatic increase in the calculated values of σ_{CT} for $\langle \varepsilon \rangle_F > 60$ eV is consistent with breakdown of the model assumptions, perhaps specifically due to the advent of other inelastic collision processes occurring in very high-E/N discharges. The similar upturn in the cross section data of Kobayashi [22] observed at lower energies in Fig. 8(a) is presumably unrelated.

All of the above analyses indicates that symmetric charge transfer is the dominant collision process affecting the transport of O_2^+ through O_2 in Townsend discharges up to 20 $\times 10^{-21}$ V m^2. The only other process which could perhaps influence the transport and flux of O_2^+ ions is collision-induced dissociation (reaction 5), but the cross section for this process is approximately 100 times smaller than for symmetric charge-exchange collisions [29].

TABLE III. Reactions affecting negative ion production and transport in a Townsend discharge in oxygen.

	Reaction	Process
7	$e + O_2 \rightarrow O^- + O$	Dissociative attachment
8	$e + O_2 \rightarrow O^+ + O^- + e$	Polar dissociation
9	$O^- + O_2 \rightarrow O_2^- + O$	Asymmetric charge exchange
10	$O_2^- + O_2 \rightarrow O_2 + O_2^-$	Symmetric charge exchange
11	$O_2^- + O_2 \rightarrow O_2 + O_2 + e$	Collisional detachment
12	$O^- + O_2 \rightarrow O + O_2 + e$	Collisional detachment

Under the discharge conditions studied here, there are no symmetric charge-exchange collisions occurring for O^+ since the concentration of atomic oxygen in the discharge due to dissociation is very small at these low currents. The only ion-molecule reaction between O^+ and O_2 that results in significant energy loss is asymmetric charge transfer (reaction 6), resulting in the destruction of O^+, and the formation of a ''slow'' O_2^+ ion. This reaction has a relatively energy-independent cross section with a magnitude about half that of reaction 4 [24,30]. This is consistent with the observation that the mean energies for O^+ exceed those of O_2^+ at all E/N [see Fig. 6(a) and Table I].

The non-Maxwellian shape of the measured distributions for O^+ is not completely understood. As mentioned above, the asymmetric charge-transfer cross section is essentially constant over the energy range of interest here, and therefore is not expected to affect the shape of the ion-flux energy distribution. It is likely that the ions are not in equilibrium at the highest values of E/N, due to the smaller collisional cross sections (compared to O_2^+) affecting their transport. This is supported by the fact that the maximum ion energies observed for O^+ approach those corresponding to the gap voltage for $E/N > 5 \times 10^{-18}$ V m^2. The ''two-temperature'' behavior at low E/N is presently unexplained.

Likewise the observed relative intensity of O^+ ions to O_2^+ ions as a function of E/N shown in Fig. 7 is also not clear. The increase with increasing E/N up to 20 $\times 10^{-18}$ V m^2 may be explained by increasing electron energies in the discharge which would favor increased dissociative ionization processes (reactions 2 and 3). However, the cause of the small decrease in relative intensity of O^+ above 20×10^{-18} V m^2 is unclear.

B. Negative ions

Listed in Table III are some of the likely collision reactions that account for the production and transport of O_2^- and O^- in the discharges studied here. Under the conditions studied here, only O^- is formed directly by interactions with electrons, i.e., by dissociative electron attachment [31] and by polar dissociation [21] (reactions 7 and 8). O_2^- may be formed by electron attachment, but that process requires electrons with energies less than 10 eV [21,31] and collisional stablization to form a stable O_2^- ion. Neither of these requirements are likely to be met at these high values of E/N, as shown by Moruzzi and Phelps [32]. The most obvious source of O_2^- is then the ion-molecule reaction 9, asymmetric charge transfer, which has a highly energy-dependent

cross section that peaks near 4 eV, and then smoothly increases with increasing ion energy above 20 eV [33–37]. The work of Moruzzi and Phelps [32] at lower E/N clearly shows the effects of asymmetric charge transfer, with O_2^- intensities beginning to exceed O^- intensities as E/N values increase beyond 300×10^{-21} V m^2 (300 Td). The decrease in the relative intensity of O^- flux to O_2^- flux with increasing E/N (Fig. 7) observed here can be attributed to the increase in cross section for reaction 9 with increasing ion energy.

The other significant ion-molecule interactions affecting the transport of the negative ions are reactions 10–12 in Table III. As with O_2^+, the transport of O_2^- is expected to be dominated by symmetric charge transfer (reaction 10) [33–35]. This is supported by the Maxwellian shape of the IFED for O_2^- at low E/N (see Fig. 4), and by the agreement between the effective cross sections calculated using the data in Table I in Eq. (3) and previous values obtained from beam experiments [Fig. 8(b)].

For E/N greater than 5×10^{-18} V m^2, the IFED's for O_2^- exhibit a non-Maxwellian shape that is manifested by a decrease in ion intensity at higher energies. This deviation is also reflected in the increase in the calculated effective cross sections shown in Fig. 8(b) at higher ion energies. This decrease in ion intensity at higher ion energies is most probably due to the destruction of O_2^- ions by collisional detachment interactions (reaction 11) whose cross sections increase with increasing ion energy [38–40].

The IFED's for O^- are highly non-Maxwellian for all E/N, indicating a complex dependence on several competing collisional processes. While the exact shapes of these distributions are not understood, and may require detailed modeling to fully characterize, it is most likely that the energy dependence of reactions 9 and 12 combine to produce the distinct shapes of the IFED's for O^-.

While the production and transport of the negative ions observed here can be reasonably well understood based upon the gas-phase reactions listed in Table III, the role of surface reactions in the formation of negative ions in oxygen discharges must also be considered. Early work in this area [41] has shown that O_2^+ ions striking a clean surface will emit O_2, O, O_2^-, and O^- particles, with the ions comprising a very small portion of the scattered beam. More recent work has shown that a beam of Na^+ ions striking a clean surface coated with oxygen produces primarily O^- ions [42]. However, Na^+ ions striking a ''dirty'' surface (i.e., a surface that has not been vacuum cleaned) coated with oxygen produces primarily O_2^- ions [43].

It is expected that a similar result would be obtained if the bombarding ions were O_2^+, which is indeed the conditions that exist in the Townsend discharges studied here. While we cannot separate the gas-phase and surface contributions to the negative ion formation, it is conceivable that both are significant, and that surface conditions may have an effect on the relative fluxes of O_2^- and O^-.

V. CONCLUSIONS

We have measured the mass and energy of the ions striking the grounded electrode of a dc Townsend discharge in oxygen over a range of E/N from 2×10^{-18} V m^2 to nearly 40×10^{-18} V m^2. The O_2^+ ion is the dominant positive ion,

while O_2^- is the dominant negative ion. Analysis of the ion-flux energy distributions indicate that a simple, one-dimensional model assuming that symmetric charge transfer is the dominate ion-molecule collision process is adequate to describe the transport of O_2^+ and O_2^- ions through the discharge for values of E/N less than 15×10^{-18} and 6×10^{-18} V m^2, respectively. Smaller, but significant, quantities of O^+ and O^- were detected with complex ion-flux energy distributions that require more sophisticated modeling to understand fully.

[1] E. W. McDaniel and E. A. Mason, *The Mobility and Diffusion of Ions in Gases* (Wiley, New York, 1973).

[2] J. L. Moruzzi and L. Harrison, Int. J. Mass Spectrom. Ion Phys. **13**, 163 (1974).

[3] R. J. Van Brunt, J. K. Olthoff, and S. B. Radovanov, in *Proceedings of the International Conference on Gas Discharges and Their Applications, Tokyo, Japan* (Chuo University, Tokyo, 1995), Vol. I, p. 486.

[4] M. Zeuner, J. Meichsner, and J. A. Rees, J. Appl. Phys. **79**, 9379 (1996).

[5] M. V. V. S. Rao, R. J. Van Brunt, and J. K. Olthoff, Phys. Rev. E **54**, 5641 (1996).

[6] J. K. Olthoff, R. J. Van Brunt, S. B. Radovanov, J. A. Rees, and R. Surowiec, J. Appl. Phys. **75**, 115 (1994).

[7] H. R. Skullerud and S. Holmstrom, J. Phys. D **18**, 2375 (1985).

[8] S. B. Radovanov, R. J. Van Brunt, J. K. Olthoff, and B. M. Jelenkovic, Phys. Rev. E **51**, 6036 (1995).

[9] E. A. Mason and E. W. McDaniel, *Transport Properties of Ions in Gases* (Wiley, New York, 1988), pp. 32–36.

[10] J. Heimerl, R. Johnsen, and M. A. Biondi, J. Chem. Phys. **51**, 5041 (1969).

[11] E. A. Den Hartog, D. A. Doughty, and J. E. Lawler, Phys. Rev. A **38**, 2471 (1988).

[12] J. K. Olthoff, R. J. Van Brunt, and S. B. Radovanov, Appl. Phys. Lett. **67**, 473 (1995).

[13] J. K. Olthoff, R. J. Van Brunt, and S. B. Radovanov, J. Res. Natl. Inst. Stand. Technol. **100**, 383 (1995).

[14] P. R. Kinsman and J. A. Rees, Int. J. Mass Spectrom. Ion Phys. **4**, 393 (1970).

[15] J. Dutton and P. Howells, J. Phys. B **1**, 1160 (1968).

[16] I. A. Fleming and J. A. Rees, J. Phys. B **2**, 423 (1969).

[17] V. H. Eiber, Z. Phys. **15**, 103 (1963).

[18] R. N. Varney, Phys. Rev. A **2**, 370 (1970).

[19] R. M. Snuggs, D. J. Volz, J. H. Schummers, D. W. Martin, and E. W. McDaniel, Phys. Rev. A **3**, 477 (1971).

[20] L. G. McKnight, Phys. Rev. A **2**, 762 (1970).

[21] Y. Itikawa, A. Ichimura, K. Onda, K. Sakimoto, K. Takay-anagi, Y. Hatano, M. Hayashi, H. Nishimura, and S. Tsurubu-chi, J. Phys. Chem. Ref. Data **18**, 23 (1989).

[22] N. Kobayashi, J. Phys. Soc. Jpn. **38**, 519 (1975).

[23] T. F. Moran, M. R. Flannery, and P. C. Cosby, J. Chem. Phys. **61**, 1261 (1974).

[24] R. F. Stebbings, B. R. Turner, and A. C. H. Smith, J. Chem. Phys. **38**, 2277 (1963).

[25] T. Baer, P. T. Murry, and L. Squires, J. Chem. Phys. **68**, 4901 (1978).

[26] S. N. Ghosh and W. F. Sheridan, J. Chem. Phys. **27**, 1436 (1957).

[27] J. A. Dillon, W. F. Sheridan, H. E. Edwards, and S. N. Ghosh, J. Chem. Phys. **23**, 776 (1954).

[28] R. F. Potter, J. Chem. Phys. **22**, 974 (1954).

[29] T. R. Moran and J. R. Roberts, J. Chem. Phys. **49**, 3411 (1968).

[30] T. F. Moran and J. B. Wilcox, J. Chem. Phys. **69**, 1397 (1978).

[31] L. G. Christophorou, Radiat. Phys. Chem. **12**, 19 (1978).

[32] J. L. Moruzzi and A. V. Phelps, J. Chem. Phys. **45**, 4617 (1966).

[33] J. A. Rutherford and B. R. Turner, J. Geophys. Res. **72**, 3795 (1967).

[34] T. L. Bailey and P. Mahadevan, J. Chem. Phys. **52**, 179 (1970).

[35] A. E. Roche and C. C. Goodyear, J. Phys. D **4**, 1513 (1971).

[36] D. Vogt, W. Dreves, and J. Mischke, Z. Naturforsch. Teil A **32**, 13 (1977).

[37] S. L. Lin, J. N. Bardsley, I. Dotan, F. C. Fehsenfeld, and D. L. Albritton, Int. J. Mass Spectrom. Ion Phys. **34**, 113 (1980).

[38] D. W. Goodson, R. J. Corbin, and L. Frommhold, Phys. Rev. A **9**, 2049 (1974).

[39] B. D. O'Neill and J. D. Craggs, J. Phys. B **6**, 2625 (1973).

[40] R. Ranjan and C. C. Goodyear, J. Phys. B **6**, 1070 (1973).

[41] P. H. F. Reijnen, A. W. Kleyn, U. Imke, and K. J. Snowdon, Nucl. Instrum. Methods Phys. Res. B **33**, 451 (1988).

[42] J. C. Tucek and R. L. Champion, Surf. Sci. **382**, 137 (1997).

[43] S. G. Walton, R. L. Champion, and Y. Wang, J. Appl. Phys. **84**, 1706 (1998).